Proceedings of the 2023 International Conference on Mathematical Physics and Computational Simulation
DOI: 10.54254/2753-8818/11/20230385

Effect of roof design on wind load of buildings through numerical simulation

Yuxin (April) Li

Groton School, Groton, MA, the USA

yli24@groton.org

Abstract. When the wind blows against a building, the resulting force acting on the building at a particular elevation is called the "wind load". Measuring and minimizing the wind load is crucial to ensure the safety of buildings. Therefore, the objective of this study is to investigate the effect of a building's roof design on the wind load by evaluating and comparing the wind pressure differences Δp that different building models experience by leveraging Computational Fluid Dynamics (CFD) simulations. The 3D CAD (Computer-Aided Design) software SolidWorks was used to construct building models of identical dimensions with the exception of roofs harboring different shapes and angles. By exerting a wind velocity through flow simulation, flow trajectories and cut plot graphs of wind velocity and pressure surrounding the building models are generated. Wind pressure differences Δp for each situation were calculated and compared based on the CFD results. Wind tunnel experimentation with building models will also executed to test the computed data and prove its reliability and applicability. The data shows that, among all tested roof designs, the barrel-vaulted roof exhibits the minimum pressure difference (of 171.15 Pa) between the windward and the leeward surface and experiences the least wind load and resists strong wind most effectively. It reduces up to roughly 15% of wind load compared to the worst case tested. For symmetric triangular gable roof designs, the greater base angle leads to greater wind load. Overall, this study provides the theoretical basis and scientific evidence for the building designs of the next generation.

Keywords: computational fluid dynamics, roof shape, wind load, pressure difference, SolidWorks, flow simulation.

1. Introduction

Background and motivation

The nature and occurrence of high winds depend on location. Studies have shown that in the United States, cities on the eastern coastline (i.e. Boston) are designated as hurricane-prone regions where high and strong winds are more likely to occur (Figure 1). Therefore, it is especially important for these cities to consider and implement strategic building designs that minimize risk incurred by high wind exposure.

DOI: 10.54254/2753-8818/11/20230385

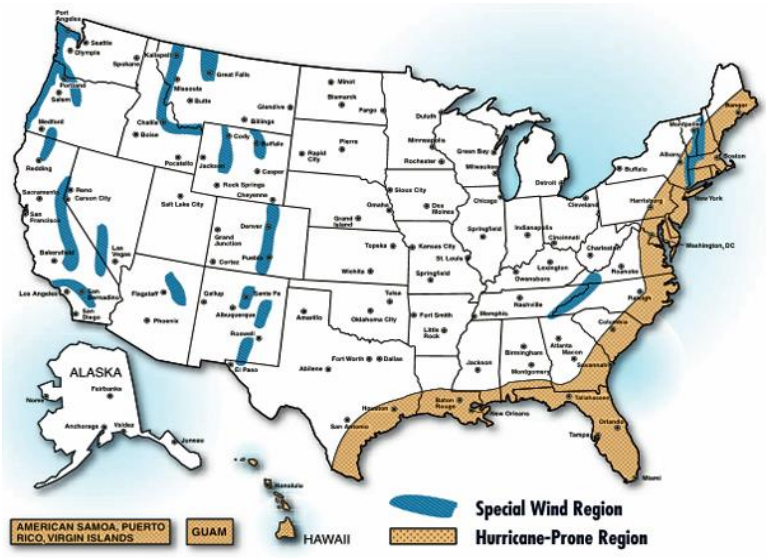

Figure 1. Hurricane-prone regions and special wind regions in the United States [1].

When the wind encounters a building, the exterior of the building experiences dynamic pressure produced by the wind. On extremely windy days, higher wind velocity leads to stronger wind pressure and greater wind load on structures; when the wind load exceeds the amount that a building is able to withstand, it can result in serious consequences such as the collapse of building components like windows, the destruction of building surfaces and even the tilting of the entire structure. In order to ensure safety, it is essential for engineers to evaluate the wind load and building designs that are able to resist wind loads, especially under hazardous weather conditions. Since the magnitude of the wind load onto a building is dependent on the shape of the building and the angle at which the wind strikes its surface, varying the building's roof to an ideal shape, size, and surface slope may effectively minimize the total wind load that the building experiences, thus significantly reducing the building's risk of tilting and sliding off. Overall, carrying out this study of evaluating and comparing the effects of the shape and surface slope of roofs on wind load will provide engineers with the optimal roof designs that can reduce the load and prevent severe damage caused by a strong wind.

1.1. Literature review

In order to reduce serious risk, multiple studies and research have been carried out by engineers to assess the relationship between a building's design and the wind load it experiences. Building elements such as the building's shape, height, and dimensions were taken into consideration. A specific study was conducted by Yuan [2], a Professor of Mechanical Engineering in Kolej University Teknikal Kebangsaan Malaysia, to test the effect of building shape on the wind pressure difference for cross-ventilation that a semi-detached low-rise building experiences through the use of Computational Fluid Dynamics simulations. By experimenting on remodelled buildings both at the windward side and the leeward side, the simulation results suggest that houses on the windward side have a 447% higher wind pressure difference than the ones on the leeward side. Thus, windward houses should have a higher cross-ventilation rate. Similarly, Meena, Raj, et. al. [3] carried out an experiment to assess and evaluate the relationship between different corner configurations of both regular and irregularly shaped buildings and wind load. After constructing four building models – two rectangular regular shaped and two irregular Y-shaped with chamfer and round corner edges – with the same cross-sectional area using ANSYS CFX, the authors compared the wind load data and illuminated that the model with a round in corner Y-shape has the minimum base moment and the minimum drag force and therefore is more aerodynamic. Another wind tunnel experiment was carried out by Cao, Tamura, and Yoshida [4] on rigid model wind pressure measurement in order to study the peak wind pressure characteristics and the effects of setbacks and parameters on medium-rise buildings that have multi-level flat roofs. Their

DOI: 10.54254/2753-8818/11/20230385

resulting data shows that simple flat roofs and multi-level flat roofs do not vary too much on the minimum negative peak pressures, but that the negative and positive extreme pressures depend heavily on step geometry. Interestingly, roofs with small tributary areas have reduced negative pressure compared to others. The present study is inspired by these experiments and adopts similar methodologies and tools to reveal novel insights.

1.2. Research scope

This study aims to discover the relationship between a building's roof design and the wind load it experiences. Computational Fluid Dynamics simulation is leveraged as a major tool in this study. Through SolidWorks, building models were constructed with identical dimensions but different types of roofs – namely flat roofs, symmetric triangular gable roofs with different base angles of 30, 45, and 60 degrees, single-slope shed roofs, and barrel-vaulted roofs. The model simulations incorporated a wind velocity of 15 m/s and wind pressure data were subsequently obtained. By comparing the wind pressure difference Δp, and the flow field for each model, I pinpointed the optimal roof design that minimizes wind load and thus reduces risk. Taking these results further, I also will execute experiments in wind tunnels with building models that are 3D-printed out through SolidWorks to verify the accuracy of these results.

2. Methodology

In this section, the governing equations controlling the fluid motions, methods of measuring wind load, and the equations utilized for calculating wind pressure differences Δp are presented to help explain the mechanism of the formation of wind load and why it is a useful and insightful parameter to measure. Mass conservation and momentum conservation are the controlling mechanisms for wind flow. Due to the complicated flow physics and building geometries, a simple formula-based calculation is inadequate to produce accurate results. Consequently, the more sophisticated CFD simulations and wind tunnel experiments are utilized here to obtain high-fidelity results.

2.1. Governing equation of mass conservation

The mass conservation states that for an arbitrary control volume, the net rate of mass increase within the volume is equal to the net mass flux into the volume. For example, in the infinitesimal control volume as shown in Fig 2, the rate of mass increase is $\frac{\partial(\rho dxdydz)}{\partial t}$. The net mass flux into the volume in x direction is the inflow rate minus the outflow rate, i.e. [5],

$$\rho v_x dydz - (\rho v_x dydz) + \frac{\partial(\rho v_x dydz)}{\partial x} dx = -\frac{\partial(\rho v_x)}{\partial x} dxdydz \tag{1}$$

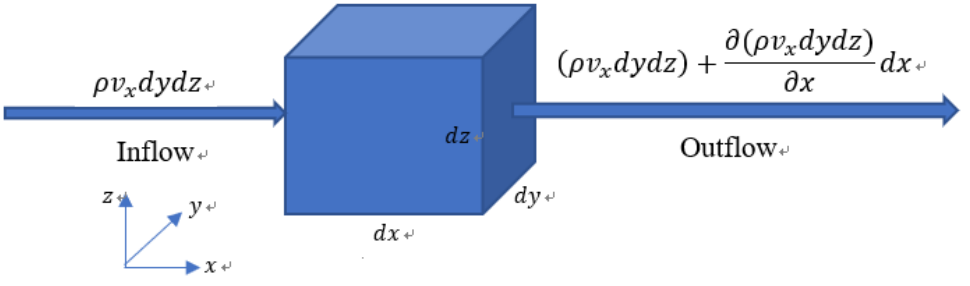

Figure 2. Taking x direction as an example in showing mass conservation in the infinitesimal control volume.

And similarly, the net mass flux into the volume in y and z directions are

$$y\ direction: -\frac{\partial(\rho v_y)}{\partial y} dxdydz \tag{2}$$

DOI: 10.54254/2753-8818/11/20230385

$$z\ direction\colon -\frac{\partial(\rho v_z)}{\partial z}dxdydz \tag{3}$$

Summing the net mass fluxes into the volume in three directions (i.e, Equation 1, 2 and 3) introduces the total net mass fluxes, which equals to the rate of mass increase in the control volume, i.e,

$$-\frac{\partial(\rho v_x)}{\partial x}dxdydz-\frac{\partial(\rho v_y)}{\partial y}dxdydz-\frac{\partial(\rho v_z)}{\partial z}dxdydz=\frac{\partial\rho}{\partial t}dxdydz \tag{4}$$

by removing the term $dxdydz$, it comes,

$$-\left[\frac{\partial(\rho v_x)}{\partial x}+\frac{\partial(\rho v_y)}{\partial y}+\frac{\partial(\rho v_z)}{\partial z}\right]=\frac{\partial\rho}{\partial t} \tag{5}$$

For the general incompressible fluid flow, which is the case of my study, the density of the fluid is a constant value, i.e., $\rho = const$, which means the rate of mass increase $\frac{\partial\rho}{\partial t}=0$, thus that the mass conservation can be expressed as,

$$\frac{\partial v_x}{\partial x}+\frac{\partial v_y}{\partial y}+\frac{\partial v_z}{\partial z}=0 \tag{6}$$

2.2. Governing equation of momentum conservation

The law of momentum conservation, which is namely a stretch of the Newton's 2nd Law, can be deduced by expanding the equation of continuity along with the Newton's 2nd law. As this is a vector relation, it can be separated into forces on each of the three dimensions. In general, the forces that anticipate, including viscosity, pressure and gravity, can be demonstrated in the following equations [5]:

$$x\text{ direction: }\rho\left(\frac{\partial v_x}{\partial t}+v_x\frac{\partial v_x}{\partial x}+v_y\frac{\partial v_x}{\partial y}+v_z\frac{\partial v_x}{\partial z}\right)=(\mu+\rho v_T)\left[\frac{\partial^2 v_x}{\partial x^2}+\frac{\partial^2 v_x}{\partial y^2}+\frac{\partial^2 v_x}{\partial z^2}\right]-\frac{\partial p}{\partial x} \tag{7}$$

$$y\text{ direction: }\rho\left(\frac{\partial v_y}{\partial t}+v_x\frac{\partial v_y}{\partial x}+v_y\frac{\partial v_y}{\partial y}+v_z\frac{\partial v_y}{\partial z}\right)=(\mu+\rho v_T)\left[\frac{\partial^2 v_y}{\partial x^2}+\frac{\partial^2 v_y}{\partial y^2}+\frac{\partial^2 v_y}{\partial z^2}\right]-\frac{\partial p}{\partial y}+\rho g_y \tag{8}$$

$$z\text{ direction: }\rho\left(\frac{\partial v_z}{\partial t}+v_x\frac{\partial v_z}{\partial x}+v_y\frac{\partial v_z}{\partial y}+v_z\frac{\partial v_z}{\partial z}\right)=(\mu+\rho v_T)\left[\frac{\partial^2 v_z}{\partial x^2}+\frac{\partial^2 v_z}{\partial y^2}+\frac{\partial^2 v_z}{\partial z^2}\right]-\frac{\partial p}{\partial z} \tag{9}$$

Here, v_x, v_y and v_z represent the velocity components in x, y, and z direction, respectively, p is the pressure, μ is viscosity, v_T is the eddy viscosity, which is determined by the k-ε model [6], and ρ is the density of the fluid. These equations are called the Navier–Stokes equations, which named after French physicist Claude-Louis Navier and Anglo-Irish physicist George Gabriel Stokes.

2.3. Assessing wind load with computational fluid dynamics and wind tunnels

Wind load is the load being exerted on the exterior of a building by the wind. Wind load is affected collectively by wind velocity, the shape of the structure, and the angle at which the wind strikes the structure. Wind load is typically categorized into three distinct types: uplift load which creates a lifting force, shear load which exerts horizontal wind pressure that leads to tilting of buildings, and lateral load which is the horizontal pushing and pulling force that causes a building to slide [7]. There are two successive methods that can effectively evaluate the wind load that a building structure experiences: Computational Fluid Dynamics (CFD) with computer simulations and wind tunnel experiment in real life.

Computational Fluid Dynamics, also called CFD, is "the art of replacing the governing partial differential equations of fluid flow" (introduced above), "with numbers and advancing these numbers in space and/or time to obtain a final numerical description of the complete flow field of interest" [5]. In short, with the aid of computers for executing complicated calculations using the governing equations, CFD calculates and predicts the wind flow while simulating the flow fields, including pressure, velocity and temperature fields, around a building structure in 3D space. In doing so, CFD successfully simulates and measures wind flow. Therefore, by utilizing SolidWorks and its flow simulation, this study

DOI: 10.54254/2753-8818/11/20230385

successfully applies CFD as a tool to perform complicated calculations, exerting wind velocity and producing flow field graphs with specific wind pressure data on each surface of the building.

Wind tunnel experiment, on the other hand, allow for the exertion of consistent, adjustable air flow. This is made possible by utilizing electric powered fans on stationary structures in order to create the same relative air movement expected in real life and measure the aerodynamic forces acting on the structure with certain devices. Images can be acquired when smoke is injected to visualize and illuminate the air flow surrounding the buildings, yielding information complementary to the flow field graphs produced by CFD. In this study, the wind tunnel experiments serve as a real-life verification and justification of the CFD-generated results, and also allow for the identification of inaccuracies in the calculations. It successfully connects the numerical simulation study to a real-life situation.

2.4. Evaluation of wind load through calculation of pressure difference

For each case of different roofs, the specific numerical wind pressure data (in numbers) on both the windward and the leeward surface of the building were generated. By subtracting the wind pressure on the leeward side $p(l)$ from the windward side $p(w)$, the total wind pressure difference Δp experienced by a given building was calculated:

$$p(w) - p(l) = \Delta p \tag{10}$$

The pressure difference caused by the wind experienced by a building is directly related to the wind load. This means that a greater pressure difference causes a heavier wind load while a smaller pressure difference causes a lighter wind load. Thus, calculating and measuring the magnitude of the pressure difference numerically represents the most intuitive method to effectively evaluate wind load.

3. Flow simulation study

This section explains the specific procedures underlying the flow simulation experiment, including how different roof shapes were designed, the 3D modeling of buildings with these designed roofs, and the simulating of wind flow and subsequent comparisons of pressure data and flow fields for the different cases.

3.1. Numerical simulation procedures

This study began by designing different types of roofs. After careful research and consideration based on existing knowledge and literature, five roof designs were selected for subsequent experiments, all of which are frequently used in real life: symmetric triangular gable roof with base angles of 30 degrees (case 1), 45 degrees (case 2) and 60 degrees (case 3), the single-sloped shed roof (case 4) and barrel-vaulted roof (case 5). Models with five different kinds of roofs are built using SolidWorks. The body dimensions were controlled for by being kept constant across all models: 10m*10m*10m (1000m^3 cubes). The single-sloped shed roof was designed to be at the same height as both the 45-degree gable roof and the barrel-vaulted roof. This resulted in the entire building standing at 15 meters high and roof height being 5 meters – these parameters were later selected for 3D-model printing in the wind tunnel experiment, as will be described later. After the models were constructed, the real wall boundary condition was added onto the surfaces, making them actual solids with the capacity to resist wind. All models are given a gravitational acceleration downward (-9.81m/s^2 in the y-direction). SolidWorks' flow simulation was then utilized to exert an air velocity of 15m/s (the condition of a windstorm) in the positive x-direction facing the slope sides of the roofs on each case. The computational domain – the region around the model where data was calculated – was set to the same size and conditions for every case as shown in Figure 3. In the x-direction, the boundaries of the domain is set to be 150m from the origin from right side and 50 m from the left side; as wind blows from left to right, the extension in length on the right side allows more calculation and observations to be made on the data of the wind after it passes by the buildings. The y direction domain boundaries are set to 75 m from the origin and 0 m since the ground blocks the wind at the ground level. In the z-direction, the domain boundaries are set to 35m and -25 m.

DOI: 10.54254/2753-8818/11/20230385

Figure 3. Computational domain set up.

Surface goals regarding the pressure on both the windward and the leeward body surfaces was set for subsequent calculations. After running the set-up and upon completion of the external flow calculation, both the contour cut plots and the flow trajectories graph of wind pressure and velocity within the computational domain were produced and recorded for each case. Specific numerical data of the windward and leeward surface pressure was exported and then taken into consideration during calculations to obtain pressure differences for each model. The graphs and the numerical data between all five cases were compared in order to inform a conclusion regarding the most ideal roof design that can effectively reduce the wind load that a building experiences in a high-wind condition. Case 2, case 4, and case 5 were selected for analysis in wind tunnel experiments and therefore were 3D-printed into actual (size-reduced) models. These models were used in the wind tunnel experiment to prove the real-life accuracy of the numerical simulation.

3.2. Building models roof designs

As explained in Section 3.1, five roof designs were chosen in this experiment and were constructed with 3-Dimentional modelling software SolidWorks. The building models face the x-z plane with the slope side of the roof in the x-direction and the front side in the z-direction. The height is in the y-direction. All five models have a body dimension of 10m*10m*10m.

The first case, as shown in Figure 4(a), is a building model with the design of a symmetric triangular gable roof with base angles of 30 degrees. The whole building has a length of 10 meters, a width of 10 meters and a total height of 12.88 meters.

The second case, as shown in Figure 4(b), is a building model with the design of a symmetric triangular gable roof with base angles of 45 degrees. The whole building has a length of 10 meters, a width of 10 meters and a total height of 15 meters.

The third case, as shown in Figure 4(c), is a building model with the design of a symmetric triangular gable roof with base angles of 60 degrees. The whole building has a length of 10 meters, a width of 10 meters and a total height of 18.66 meters.

The fourth case, as shown in Figure 4(d), is a building model with the design of a single-sloped shed roof. The surface with the slope of the roof is the windward side, facing the negative x-direction. The whole building has a length of 10 meters, a width of 10 meters and a total height of 15 meters.

The fifth case, as shown in Figure 4(e), is a building model with the design of a barrel-vaulted (round) roof. The whole building has a length of 10 meters, a width of 10 meters and a total height of 15 meters.

DOI: 10.54254/2753-8818/11/20230385

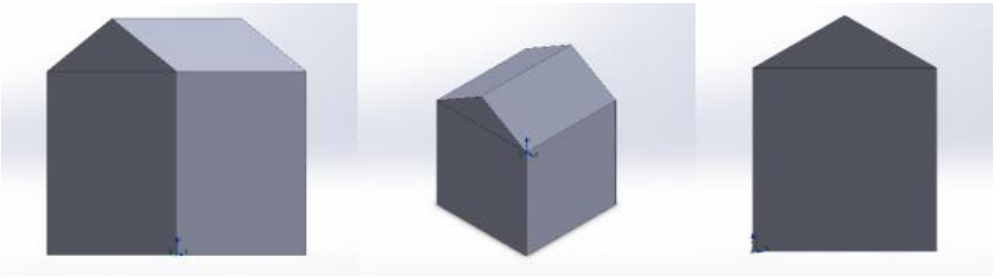

(a)

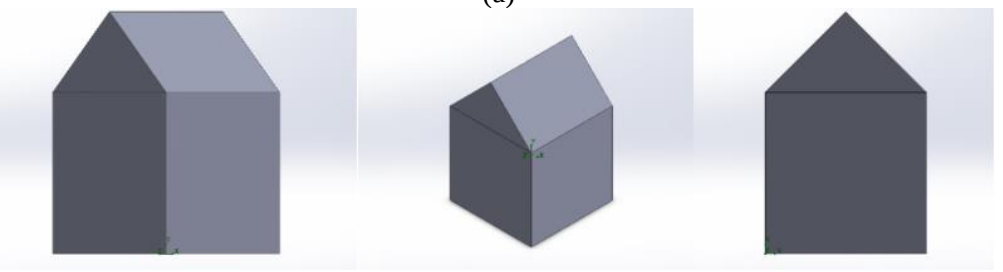

(b)

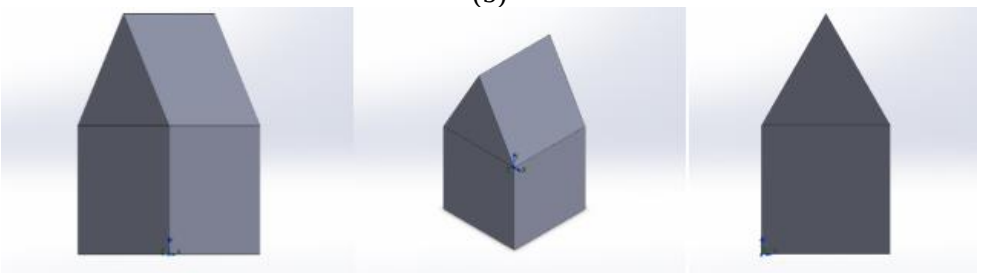

(c)

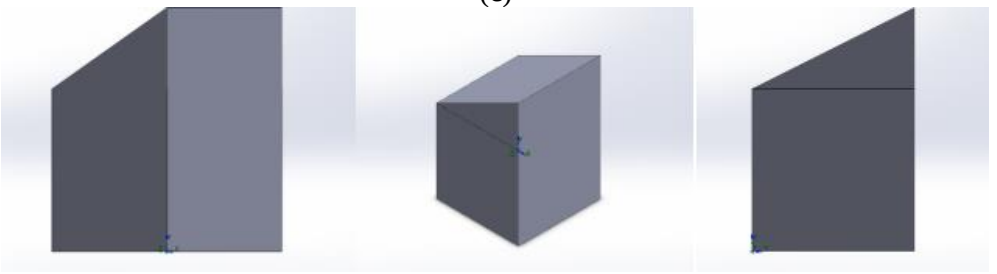

(d)

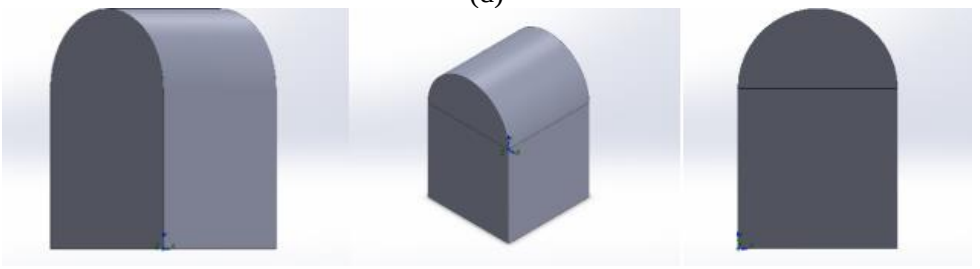

(e)

Figure 4. Building models from different perspectives. (a) Building model with symmetric triangular gable roof with base angles of 30 degrees (case 1) from different perspectives; (b) Building model with symmetric triangular gable roof with base angles of 45 degrees (case 2) from different perspectives; (c) Building model with symmetric triangular gable roof with base angles of 60 degrees (case 3) from different perspectives; (d) Building model with single-sloped shed roof (case 4) from different perspectives; (e) Building model with barrel-vaulted (round) roof (case 5) from different perspectives.

DOI: 10.54254/2753-8818/11/20230385

After numerical simulations, results were generated including pressure and velocity data in the form of numerical data, cut plots, and flow trajectories graphs of all five models. Comparisons were then executed to identify the optimal model.

3.3. Pressure difference comparisons of the pressure on two sides

The results in Table 1 represent the outcome of the calculations based on the surface goal being set for the pressure difference on both the windward and the leeward side of each building model.

Table 1. Simulation results of pressure on windward and leeward building surfaces which is further used to evaluate pressure difference.

Case No.	Windward pressure (Pa)	Leeward pressure (Pa)	Pressure Difference Δp (Pa)
1	101361.3289	101186.7115	174.62
2	101360.9109	101144.0855	216.83
3	101358.8985	101112.5712	246.33
4	101361.4761	101156.0322	205.44
5	101364.094	1011192.9486	171.15

The data shows that the windward surface experiences a higher wind pressure compared to the leeward surface of the building with a high value in Pa; the difference between the two surfaces creates a pressure difference on each building model. By comparing all five sets of data, the results show that case 5 (barrel-vaulted roof) has the smallest pressure difference of 171.15 Pa. Thus, case 5 experiences the smallest wind load. Case 1 (symmetric triangular gable roof with base angle of 30 degrees) has the second smallest pressure difference of 174.62 Pa, around 2.03% greater than case 5. Case 4 (single-sloped shed roof) is 17.65% greater than case 1, with a pressure difference of 205.44 Pa. After that, case 2 exhibits a pressure difference of 216.83 Pa, about 11.98% smaller than case 3, which has the greatest wind pressure difference of 246.33 Pa. Equipped with all the numerical data, it is now evident that the order of the 5 cases (from the smallest to the greatest wind pressure difference and thus the smallest wind load to the greatest wind load) is: case 5 < case 1 < case 4 < case 2 < case 3. The results also demonstrate that the data differences observed in case 5 and case 1 is relatively small while the data difference between case 4, 2 and 3 are larger. For each case, both the pressure contour cut plots and the pressure flow trajectories graph are recorded and presented below.

3.4. Pressure field comparison

For each case, the pressure contour cut plots are recorded and presented below in Figure 5, wherein the colour scale is set identically from 100443.00 Pa (lowest, represented by dark blue) to 101410.00 Pa (highest, represented by red). It is apparent that, for all cases, as the wind hits from the left to the right, a higher pressure is formed at a lower elevation and decreases as the elevation increases. At the elevation of the building, a high-pressure front region is formed in front of the building on the windward surface, while a lower back pressure region is created at the back of the building on the leeward surface.

DOI: 10.54254/2753-8818/11/20230385

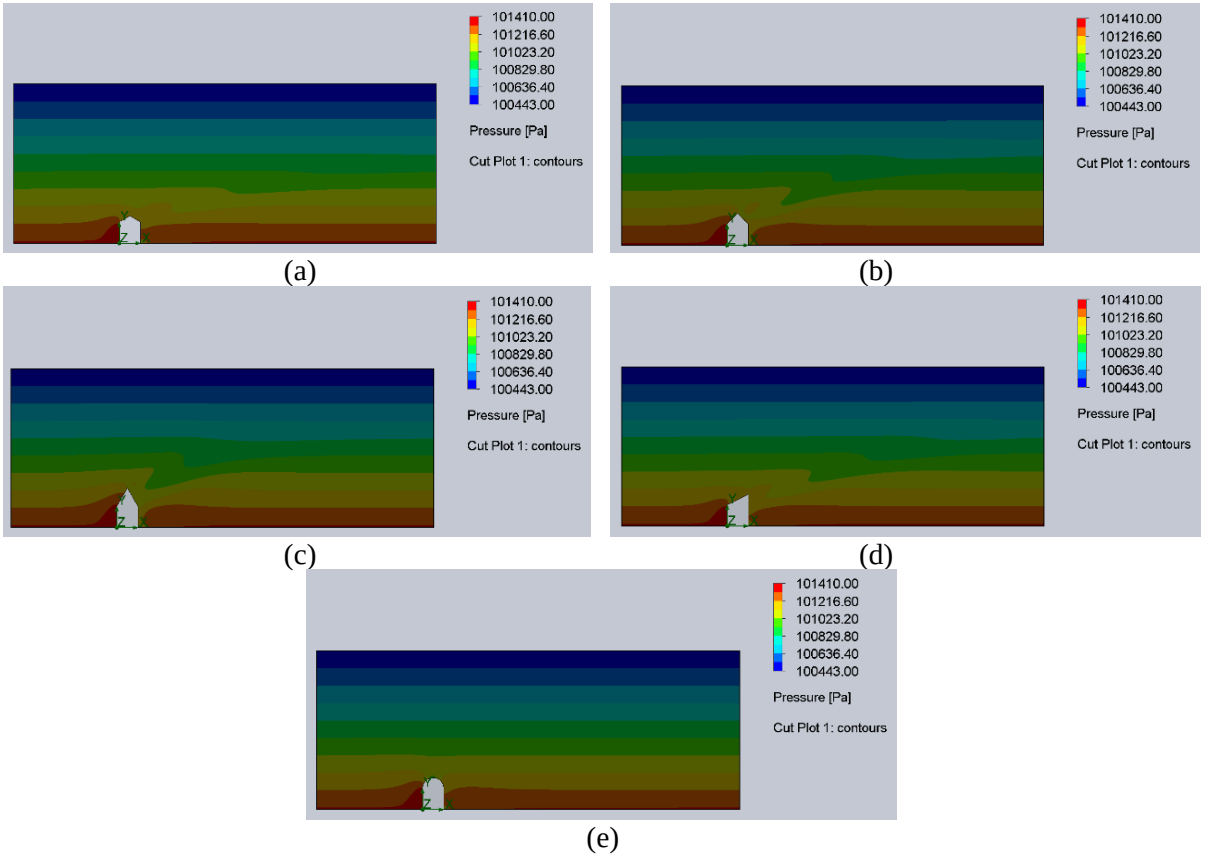

Figure 5. Pressure contour cut plot for five cases: (a) case 1, (b) case 2, (c) case 3, (d) case 4, (e) case 5.

For all five graphs, the high-pressure area on the windward side looks similar as a red region rises to the building's body. The region above the red is also affected as all rises by a small amount except for case 5, where the region above the building model is nearly not affected at all. This suggests that among all five cases, case 5 has the lowest pressure above the building body and maintains a relatively steady pressure contour both in front and above the model. Case 3 has the greatest red (roughly 101400.00 Pa) and dark orange (roughly 101300.00 Pa) area in front of the building. At the back of the building on the leeward side, the light orange region covers more surface for case 2, 3 and 4, indicating that these two cases possess a lower back pressure than the other 3 cases, which result in a greater pressure difference. Case 1 and 5 both have a relatively greater dark orange region at the back, suggesting that their back-pressure regions exhibit higher pressure compared to their other regions, which is closer to the front pressure. Collectively, these observations obtained from the pressure contour graphs prove that case 5 has the least pressure difference and that case 3 has the greatest. Therefore, case 5 should experience the least wind load among all five cases.

3.5. Pressure flow trajectories comparisons

In order to further visualize the pressure in the field and to explain the its behaviour, the flow trajectories are included in Figure 6.

DOI: 10.54254/2753-8818/11/20230385

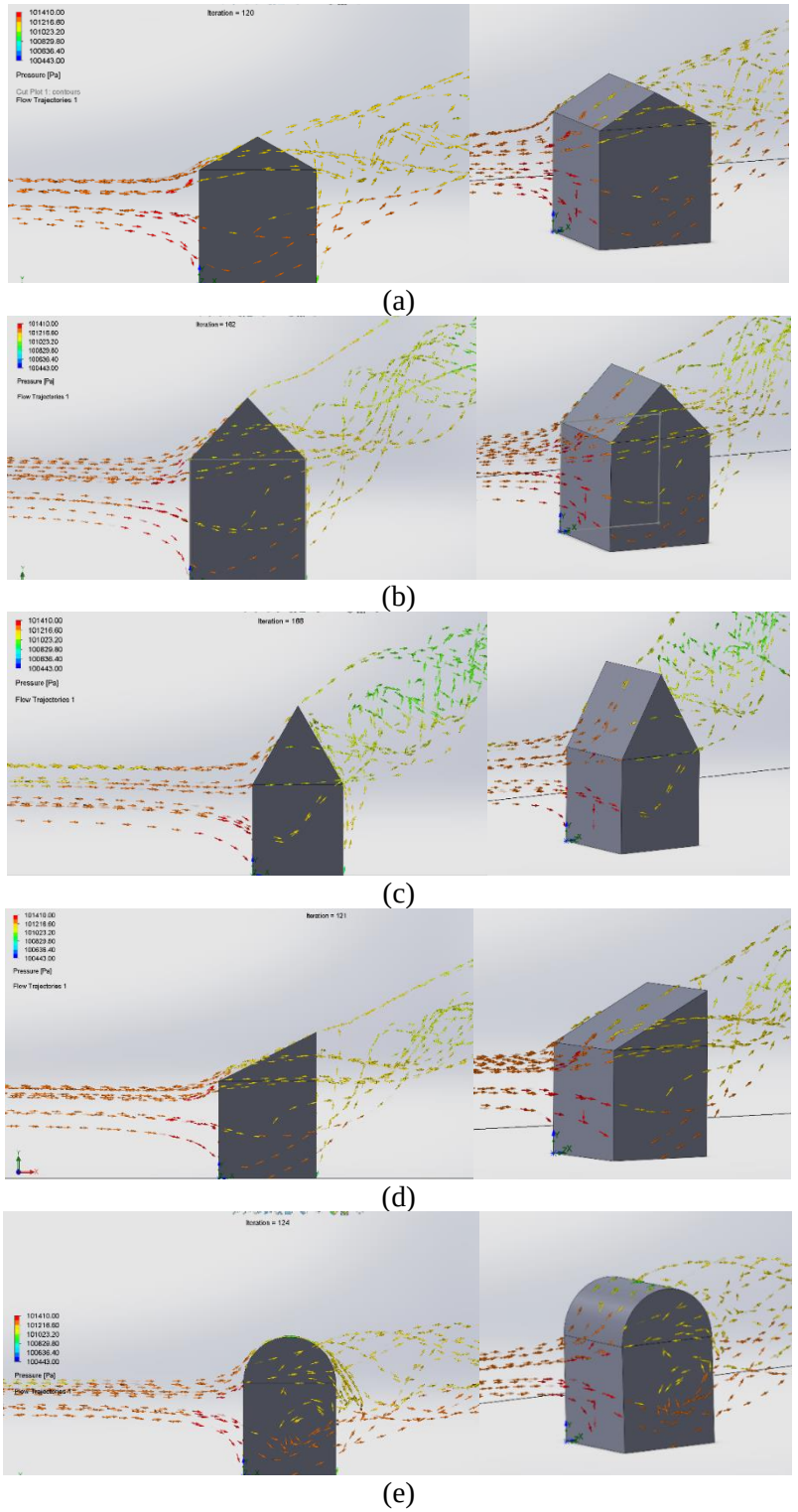

Figure 6. Pressure flow trajectories for five cases: (a) case 1, (b) case 2, (c) case 3, (d) case 4, (e) case 5.

In the flow trajectories graphs for all five cases, the arrows represent the direction (as vectors) and the magnitude (represented by the colour scale) of the pressure in the field. This, in turn, is indicative of the wind flow and pressure changes around the building models. The flow trajectories graph for Case 5 validates the previous observations from the cut plot since the pressure surrounding the building model is affected least and remains the steadiest compared to all other cases. Specifically, this is evident

DOI: 10.54254/2753-8818/11/20230385

because the flow of arrows rises the least at the leeward side and has the smallest change in colour (mostly red and orange, which is similar to the colour at the front). In contrast, other cases experience a significant change in flow elevation and magnitude, as exemplified by the arrows' colours. Case 3, in particular, exhibits the greatest rise of the flow and the greatest colour differences which span from red to green (101410 Pa to roughly 101000 Pa). This suggests that case 3 is the least steady and experiences the greatest pressure difference (shown by the greatest change in colour). All observations from the flow trajectories graphs agree with the previous conclusions and the numerical pressure difference data obtained and described previously.

3.6. Velocity field comparisons

For each case, the velocity contour cut plots are recorded and presented below.

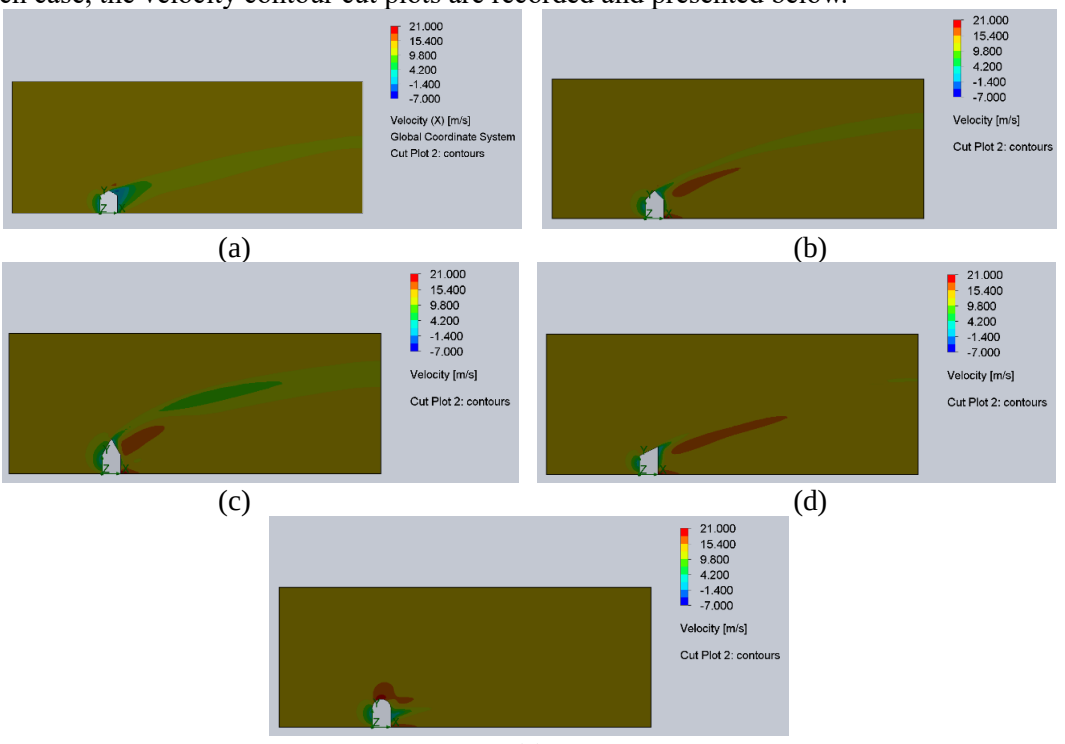

Figure 7. Velocity contour cut plot for five cases: (a) case 1, (b) case 2, (c) case 3, (d) case 4, (e) case 5.

Based on all of the velocity contour cut plots shown in Figure 7, the colour scale is set identically from -7m/s (lowest, represented by dark blue) to 21.00 m/s (highest, represented by red). For all cases, most of the regions around the building have a yellowish-orange colour, indicating that the wind velocity is roughly around 14-15 m/s, which is the speed set up for the simulation. As the wind hits from the left to right, a light yellow and green area is formed in front of the building on the windward surface, which is a lower wind velocity around 4.20 to 9.80 m/s.

For case 2, 3, and 4, a higher wind velocity area is created behind the building and increases in elevation as it goes further away from the building, reaching a velocity of over 20.00 m/s as indicated by the red colour. Case 1, 2, and 3 also have a similar area of lower wind velocity created behind the building. Case 5, on the other hand, remains steady and has nearly no change of wind velocity behind the building compared to the bigger environment. It has a high wind velocity over 20.00 m/s on the top of the roof but not on the leeward surface. The high velocity over the top of the roof indicates that the wind is able to flow smoothly over the building instead of being fully or partially inhibited, which would have increased the pressure and force acting on the surface. One can readily observe that only a very small area of green is located at the back of the structure. Collectively, these observations suggest that case 5 has the steadiest condition.

DOI: 10.54254/2753-8818/11/20230385

3.7. Velocity flow trajectories comparisons

In order to further visualize the velocity flow in the field and explain its behaviour, flow trajectories were generated and are presented in Figure 8.

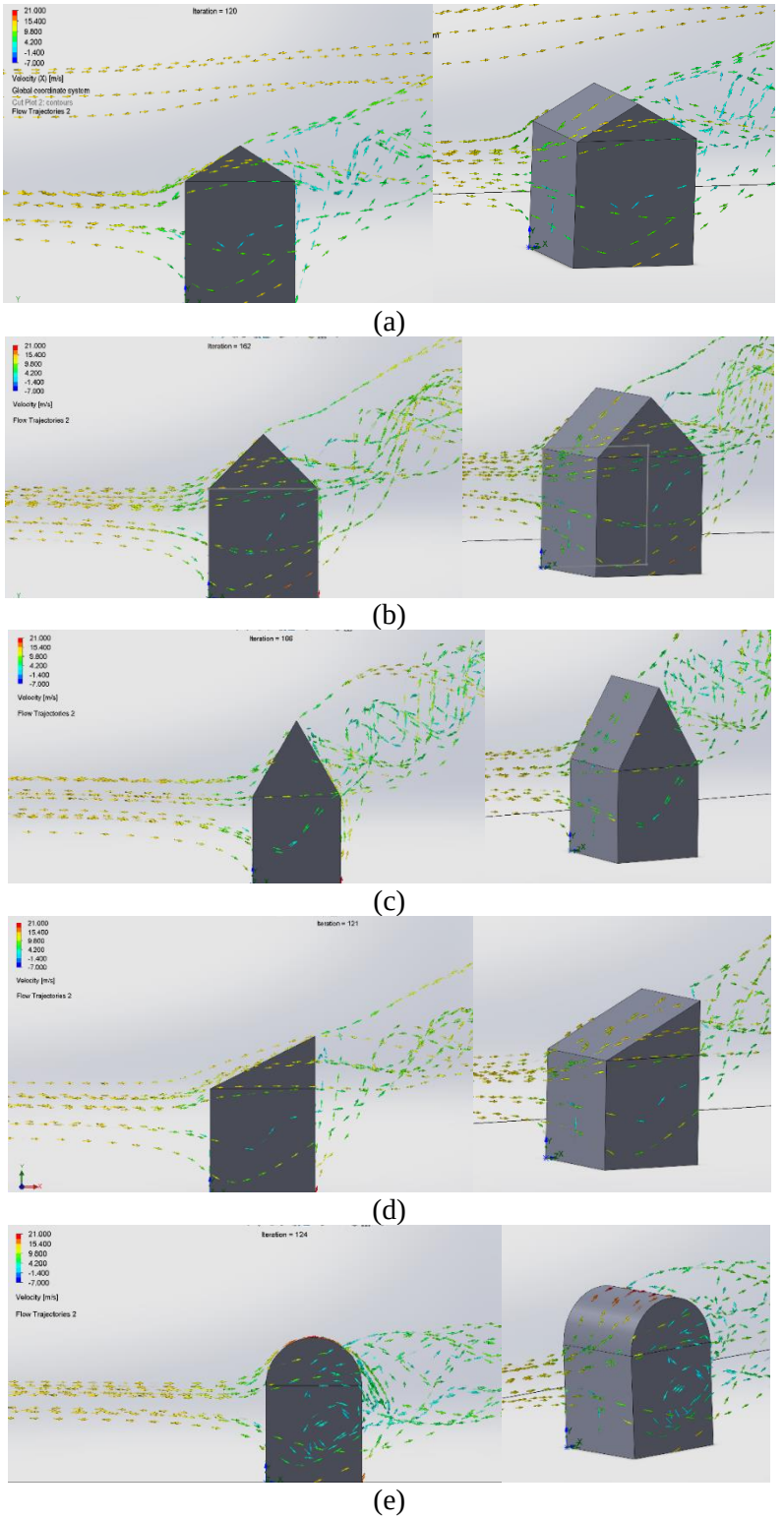

Figure 8. Velocity flow trajectories for five cases: (a) case 1, (b) case 2, (c) case 3, (d) case 4, (e) case 5.

DOI: 10.54254/2753-8818/11/20230385

Conceptually similar to the flow trajectories graphs generated for pressure, the velocity flow trajectories graphs have arrows that indicate the wind flow and changes in wind velocity around the building models. The rise of the elevation of the arrows' flow for velocity and pressure is consistent with those of the flow trajectories graphs generated for pressure. Indeed, case 5 rises least and case 3 rises most. In case 5's flow trajectories graph, there is a black flow of the wind velocity on the surface of the building model, which is a factor that contributes to a higher pressure on the back and thus reduces the pressure difference. In addition, case 5 and case 1 have the most arrows with tiffany blue (indicative of roughly 2.00 m/s) at the leeward side compared to the other cases, which exhibit mostly green arrows (indicative of roughly 7.00 m/s). This suggests that the wind velocity behind the building model for case 5 and case 1 is relatively smaller than that of the other cases. This, in turn, causes the wind pressure difference to decrease and results in a steadier environment around the building. Moreover, akin to the observations derived from the velocity contour cut plot, case 5 has a high wind velocity over the top of the roof (represented by the colour red of roughly 20.00 m/s). This may have been caused by the round and thus smooth and aerodynamic surface of the roof, which theoretically allows wind to flow smoothly over the top, thus reducing pressure and force as it encounters the surface.

3.8. Windward and leeward surface pressure contour graph comparisons

Based on the previous data and graphs collected, case 5 with the round roof has the best performance while case 3 with the 60-degree gable roof has the worst performance. For the purpose of better visualizing the pressure on both the windward side and the leeward side and the differences between these two cases, surface pressure contour graphs were recorded and presented in Figure 9 and 10.

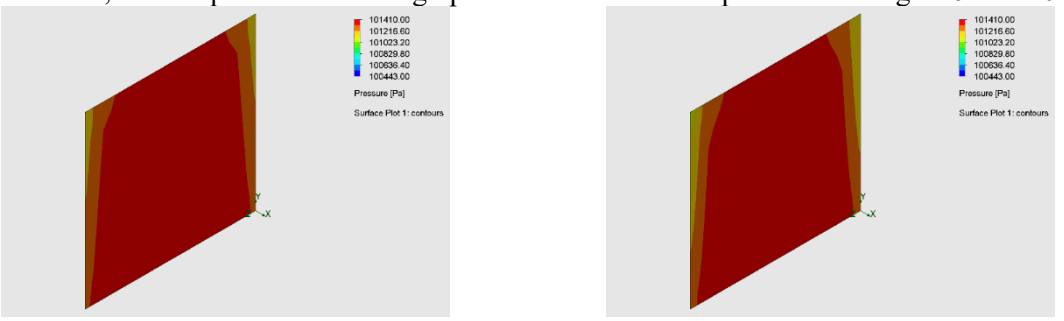

(a) (b)

Figure 9. Windward Surface Pressure Contour graphs comparison: (a) case 5 with round roof, (b) case 3 with 60-degree triangular gable roof.

According to Figure 9, for both cases, a large area of red appears on the windward surface, indicating a large pressure based on the colour scale. The two graphs look almost identical, with a small area of orange and yellow on the sides and top corners. This suggests that case 5 and case 3 have similar magnitude and distribution of wind pressure on the windward side of the buildings, with the highest pressure in the centre and the lowest pressure on the sides.

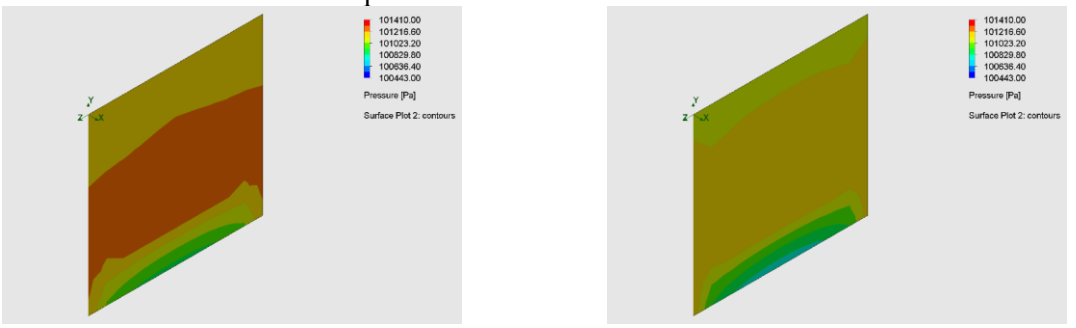

(a) (b)

Figure 10. Leeward Surface Pressure Contour graphs comparison: (a) case 5 with round roof, (b) case 3 with 60-degree triangular gable roof.

DOI: 10.54254/2753-8818/11/20230385

On the other hand, Figure 10 demonstrates a bigger difference between two cases on the leeward surface. Both cases have the largest wind pressure in the middle section of the surface, presented by red and yellow, and the smallest wind pressure at the bottom of the surface, presented by green. However, almost half of the surface displays red for case 5 while case 3 shows no red at all, implying that case 5 has a much larger wind pressure on the leeward surface compared to that of case 3.

Since two cases have identical windward surface pressure but that case 5 has a significantly greater pressure compared to case 3 on the leeward side, it proves that case 5 should have a smaller pressure difference between the windward and the leeward surface than case 3. This also suggests that roof design barely affects the wind pressure on the windward side as the wind first approaches the building, but it considerably affects the wind pressure on the leeward side, after the wind blows and passes by the building.

4. Wind tunnel experiment

In this section, the wind tunnel experiment was carried out with wind tunnels, a measuring device, camera and 3D models that are printed out with a 3D printer using the models previously constructed on SolidWorks. The same wind velocity, generated by the tunnels, was exerted on three models with different roofs. Images were acquired for subsequent analyses.

4.1. Three-dimensional printing of building models

Three of the building models developed in Section 3 (case 2, case 4 and case 5) were selected for further analyses utilizing 3D printing and subsequent wind tunnel experiments. The 3D-printed building models are shown in Figure 11.

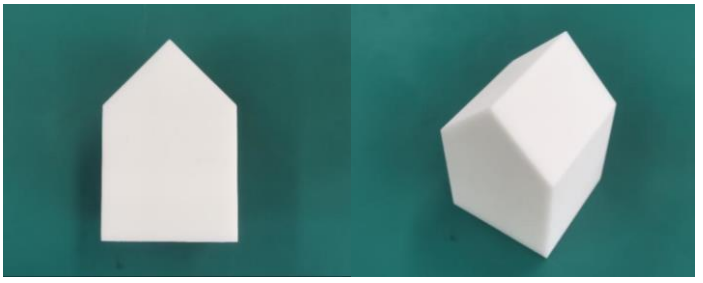

(a)

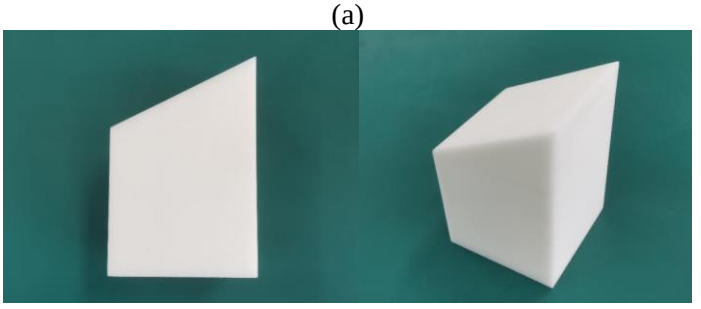

(b)

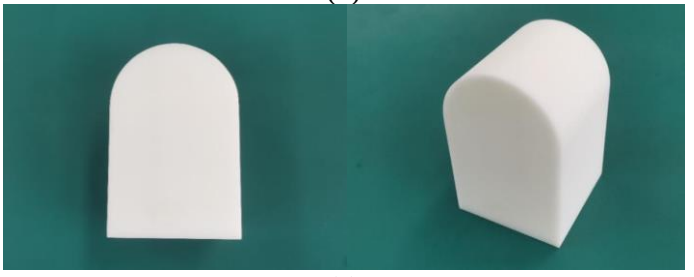

(c)

Figure 11. 3D printed building models: (a) case 2 with symmetric triangular gable r=roof, (b) case 4 with single-sloped shed roof, (c) case 5 with barrel-vaulted roof.

DOI: 10.54254/2753-8818/11/20230385

4.2. Experiment procedures

This subsection details the procedures of the wind tunnel experiments.

a. 3D model printing

1. Adjust the SolidWorks models according to the scale of 100:1 and print the building models with 3D printer in the size of 10cm*10cm*10cm.

b. Visualization of building flow field

2. Use small wind tunnel equipment (Equipment: wind tunnel; Brand: Armfield, Model: C15-10) to simulate the wind around the house.

3. Put the 3D printed model into the wind tunnel, then open the wind tunnel and adjust the wind speed to 15m/s.

4. Open the accessories of the smoke generating device and heat the glycerol to produce smoke traces in order to allow the flow traces to float with the airflow.

5. Simulate the airflow streamline to display the flow field around the model.

6. Observe and record the smoke traces around the house.

7. Replace the model in the same way to continue the test.

c. Pressure test on the windward/leeward side of the building

8. Drill a 2mm diameter hole on the windward/leeward surface of the model and connect the gas pressure sensor pipeline.

9. Put the building models into the wind tunnel, then open the wind tunnel and adjust the wind speed to 15m/s.

10. measure the pressure on the windward/leeward surface of the building.

11. Repeat the test for 3 times.

12. Replace the model in the same way and continue to complete the test.

The equipment used for the wind tunnel experiment (Armfield, Model: C15-10) is shown in Figure 12.

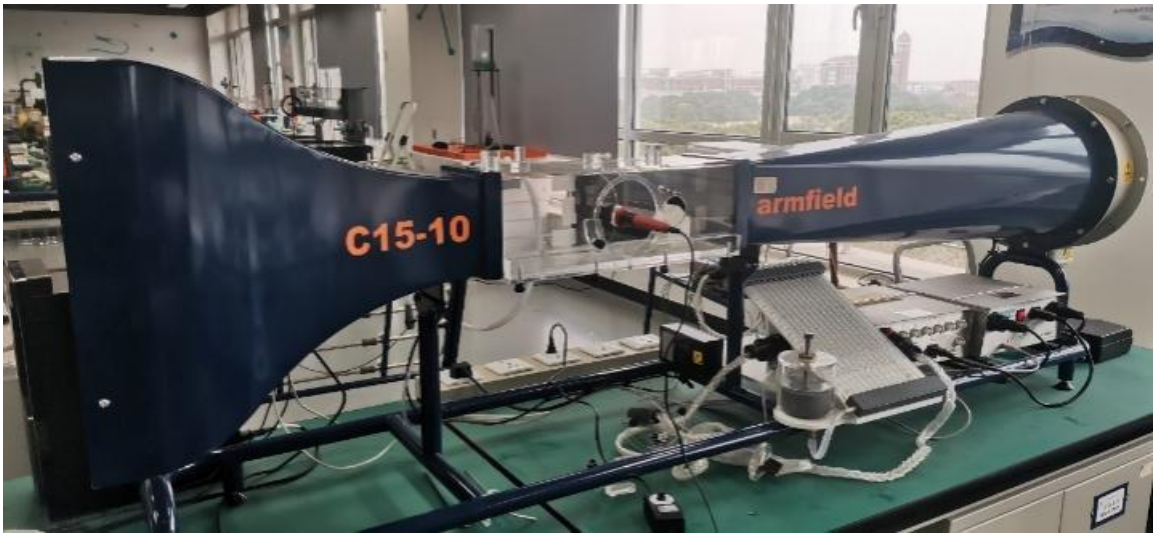

Figure 12. Wind tunnel Armfield, Model: C15-10.

The experimental and the data collection approach is shown in Figure 13.

DOI: 10.54254/2753-8818/11/20230385

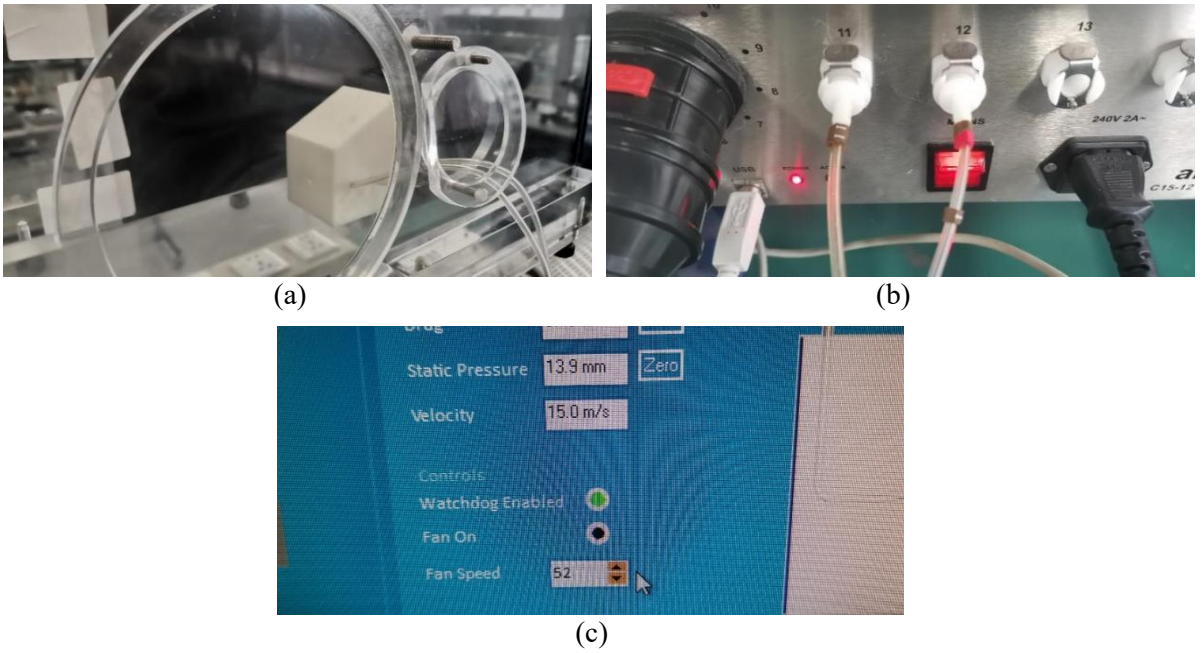

(a) (b)

(c)

Figure 13. Pressure measurements for the windward/leeward sides of the building (a) sensors at the building, (b) pressure is linked to the computer, (c) the data collection and recording system.

4.3. Results and analysis

The results of wind tunnel experiments are presented in Table 2. These data reveal that, among the 3 tested cases, the barrel-vaulted roof exhibits the best performance with a pressure difference of 158.00 Pa. This is less than the wind pressure difference of the symmetric triangular gable roof (172.67 Pa) and the wind pressure difference of the single-sloped shed roof (200.67 Pa). Further comparisons of the results from the simulations and wind tunnel experiments demonstrated that both approaches showed that barrel-vaulted roofs have the best performance. Thus, we conclude that this is the optimal design. This conclusion has important implications – hurricane-prone regions and special wind regions should design buildings with barrel-vaulted roofs. In contrast, the other two cases tested (symmetric triangular gable roof and single-sloped shed roof) exhibited slight pressure differences between the simulations and wind tunnel experiments, which may have been caused by the settings of the numerical simulations.

Table 2. Wind tunnel experiment results.

Case No.	Test	Windward pressure (Pa)	Leeward pressure (Pa)	Δp (Pa)	Averaged Δp (Pa)
Case 2-symmetric triangular gable roof	1	101317	101144	173	172.67
	2	101315	101154	161	
	3	101316	101132	184	
Case 4-single-sloped shed roof	1	101314	101099	215	200.67
	2	101317	101124	193	
	3	101318	101124	194	
Case 5- barrel-vaulted roof	1	101314	101157	157	158.00
	2	101315	101165	150	
	3	101314	101147	167	

DOI: 10.54254/2753-8818/11/20230385

5. Conclusion and future work

5.1. Conclusion

The objective of this study was to investigate the effect of roof design on the wind load that a building experiences in order to find the most ideal roof that can effectively minimize the load. Numerical simulations show that under the same conditions, the building model with a barrel-vaulted roof (case 5) experiences the smallest wind pressure difference of 171.15 Pa, which is 1.99% less than the building model with a symmetric triangular gable roof with a base angle of 30 degrees (case 1), which undergoes the second smallest wind pressure difference of 174.62 Pa. Case 3 (the building model with a symmetric triangular gable roof with a base angle of 60 degrees) experiences the greatest wind pressure difference of 246.33 Pa, 13.61% more than case 2 (the building model with a symmetric triangular gable roof with a base angle of 45 degrees), which undergoes the second greatest wind pressure difference of 216.83 Pa. Among the three cases with symmetric triangular gable roofs harbouring different base angles, the case with a 30-degree angle exhibits the smallest load while the case with a 60-degree angle exhibits the greatest load. These three cases suggest that the greater the base angle of the symmetric triangular gable roof, the greater wind pressure difference on the building. On the other hand, among cases 2, 4, and 5, the wind tunnel experiment shows that case 5 undergoes the least wind pressure difference of 158.00 Pa, which agrees with the results from the CFD numerical simulation. Case 4 undergoes the greatest wind pressure difference of 200.67 Pa and case 2 has a wind pressure difference of 172.67 Pa.

Overall, building model with a barrel-vaulted roof, as shown both by the CFD simulation and the wind tunnel experiment results, is considered to be the most ideal roof design that can best help the building to resist strong wind and reduce risks of sliding and tilting.

5.2. Future work

In the future, I aim to further investigate the effect of roof design and roof levels on higher building models that will become more common in big cities in the future for offices and apartments. In addition, I would also like to assess the effect of building shapes on the wind load, including cases such as rectangular (greater height or greater length), cylindrical, domed, and triangular body shapes. Under the condition of increasing the public pursuit of architectural aesthetics, these building shapes will be used more often by architects. Therefore, I believe that this study will be very helpful for engineers while constructing buildings.

References

[1] FEMA. (2010). Wind retrofit guide for residential buildings. FEMA P-804. Washington, DC:FEMA.

[2] Yuan, C. S. (2007). The effect of building shape modification on wind pressure differences for cross-ventilation of a low-rise building. International Journal of Ventilation, 6(2), 167-176.

[3] Meena, R. K., Raj, R., & Anbukumar, S. (2022). Effect of wind load on irregular shape tall buildings having different corner configuration. Sādhanā, 47(3), 1-17.

[4] Cao, J., Tamura Y.,& Yoshida A. (2012) Effect of Setback and Its Parameter on Peak Wind Pressures on Multi-Level Flat Roofs, 31(9), 1-8.

[5] Munson, B. R., Okiishi, T. H., Huebsch, W. W., & Rothmayer, A. P. (2013). Fluid mechanics. Singapore: Wiley.

[6] Tominaga, Y., & Stathopoulos, T. (2009). Numerical simulation of dispersion around an isolated cubic building: comparison of various types of k–ε models. Atmospheric Environment, 43(20), 3200-3210.

[7] Wendt, J. F. (Ed.). (2008). Computational fluid dynamics: an introduction. Springer Science & Business Media. 5-6.